Reporter nanoparticle that monitors its anticancer efficacy in real time

Ashish Kulkarni[a,b,1], Poornima Rao[a,b], Siva Natarajan[a,b], Aaron Goldman[a,b], Venkata S. Sabbisetti[c], Yashika Khater[a,b], Navya Korimerla[a,b], Vineethkrishna Chandrasekar[a,b], Raghunath A. Mashelkar[d,1], and Shiladitya Sengupta[a,b,e,1]

[a]Laboratory of Nanomedicine, Harvard–Massachusetts Institute of Technology Division of Health Sciences and Technology, Harvard Medical School, Boston, MA 02115; [b]Division of Biomedical Engineering, Harvard Medical School, Boston, MA 02115; [c]Division of Renal (Kidney) Medicine, Department of Medicine, Brigham and Women's Hospital, Harvard Medical School, Boston, MA 02115; [d]National Chemical Laboratory, Pune 411008, India; and [e]Dana Farber Cancer Institute, Boston, MA 02115

Contributed by Raghunath A. Mashelkar, March 4, 2016 (sent for review May 30, 2015; reviewed by Anirban Maitra and Weian Zhao)

The ability to monitor the efficacy of an anticancer treatment in real time can have a critical effect on the outcome. Currently, clinical readouts of efficacy rely on indirect or anatomic measurements, which occur over prolonged time scales postchemotherapy or postimmunotherapy and may not be concordant with the actual effect. Here we describe the biology-inspired engineering of a simple 2-in-1 reporter nanoparticle that not only delivers a cytotoxic or an immunotherapy payload to the tumor but also reports back on the efficacy in real time. The reporter nanoparticles are engineered from a novel two-staged stimuli-responsive polymeric material with an optimal ratio of an enzyme-cleavable drug or immunotherapy (effector elements) and a drug function-activatable reporter element. The spatiotemporally constrained delivery of the effector and the reporter elements in a single nanoparticle produces maximum signal enhancement due to the availability of the reporter element in the same cell as the drug, thereby effectively capturing the temporal apoptosis process. Using chemotherapy-sensitive and chemotherapy-resistant tumors in vivo, we show that the reporter nanoparticles can provide a real-time noninvasive readout of tumor response to chemotherapy. The reporter nanoparticle can also monitor the efficacy of immune checkpoint inhibition in melanoma. The self-reporting capability, for the first time to our knowledge, captures an anticancer nanoparticle in action in vivo.

nanoparticle | immunotherapy | monitoring | chemotherapy | reporter

The failure of anticancer therapy is a major cause of mortality (1). Although the current dogma underlying resistance is based on the Darwinian selection of mutations acquired over time under chemotherapy pressure, emerging evidence indicates that anticancer drugs can be rendered ineffective early on by intrinsic or adaptive resistance as a function of tumor heterogeneity (2–4). For example, response rates to first-line chemotherapy treatments in metastatic breast cancer patients range from a dismal 30% to 70%, and patients with disease progression need to be switched to a different drug (5). Similarly, about 40–60% of patients with a wild-type KRAS do not respond to cetuximab (6). The ability to detect early whether a treatment is working or not and to switch, if necessary, to a regimen that is effective can have a significant effect on the outcome as well as quality of life (7, 8).

Currently, tumor response to therapy is determined using techniques for direct anatomical measurements, such as computed tomography (CT) and magnetic resonance imaging, or indirectly using positron emission tomography with 2-[fluorine-18]fluoro-2-deoxy-d-glucose (FDG-PET) to quantify metabolic activity. However, these techniques lack the sensitivity or specificity to enable very early response assessment, and often, clinicopathological and metabolic readouts can be discordant (5, 9, 10). In the case of immunotherapy, for example, a productive immune response (T cell infiltration) and the unimpeded growth of the tumor will both be manifest as progression on the conventional Response Evaluation Criteria in Solid Tumors (RECIST) criteria, but the biological underpinnings are 180° apart (11). We reasoned that the optimal strategy to overcome these limitations is to directly capture the outcome of chemotherapy or immunotherapy activity in the tumor in real time. We rationalized that a smart material could not only exert an antitumor effect but also facilitate the early visualization of efficacy in vivo.

Intelligent, designed nanoscale materials are increasingly being engineered for applications in cancer management (12). For example, early studies on the application of nanomaterials in cancer focused on the delivery of chemotherapy agents to the tumor (13, 14). Recent studies have shown that rationally engineered polymers and pathophysiology-inspired nanomaterials can enhance the efficacy of chemotherapy agents (15–18). Multiple cancer nanomedicines are currently in the clinics (19). In parallel, nanomaterials have been developed as probes for fluorescent, optical, Raman, and magnetic resonance imaging of the tumor (20–23). The use of dual-emissive materials or stimuli-responsive nanomaterials has further advanced the imaging modality to the molecular level by conferring the ability to monitor subcellular and microenvironment changes, such as hypoxia or pH transitions (24, 25). Similarly, tumor-activatable nanoparticles were used to detect metastasis and residual tumor (26). The emerging paradigm is the development of nanomaterials that integrate both the imaging and therapeutic capabilities into single systems, termed theranostics, which allow the tracking of drug delivery to tumor or image-guided tumor ablation (27, 28). For example, in a recent study, nanodendrons were engineered to carry a near-infrared imaging beacon that allowed the tracking of the nanoparticle and additionally deliver

Significance

The ability to identify responders and nonresponders very early during chemotherapy by direct visualization of the activity of the anticancer treatment and to switch, if necessary, to a regimen that is effective can have a significant effect on the outcome as well as quality of life. Current approaches to quantify response rely on imaging techniques that fail to detect very early responses. In the case of immunotherapy, the early anatomical readout is often discordant with the biological response. This study describes a self-reporting nanomedicine that not only delivers chemotherapy or immunotherapy to the tumor but also reports back on its efficacy in real time, thereby identifying responders and nonresponders early on.

Author contributions: A.K., R.A.M., and S.S. designed research; A.K., P.R., S.N., A.G., V.S.S., Y.K., N.K., and V.C. performed research; A.K., P.R., S.N., A.G., V.S.S., R.A.M., and S.S. analyzed data; and A.K., R.A.M., and S.S. wrote the paper.

Reviewers: A.M., University of Texas MD Anderson Cancer Center; and W.Z., University of California, Irvine.

The authors declare no conflict of interest.

[1]To whom correspondence may be addressed. Email: ashishk@mit.edu, ram@ncl.res.in, or shiladit@mit.edu.

This article contains supporting information online at www.pnas.org/lookup/suppl/doi:10.1073/pnas.1603455113/-/DCSupplemental.

www.pnas.org/cgi/doi/10.1073/pnas.1603455113

Downloaded at Palestinian Territory, occupied on December 12, 2021

www.manaraa.com

a therapeutic that was activated inside the tumor by matrix metalloproteinase enzymes and thereby reduced off-target toxicity (29).

However, despite the advances in the use of nanomaterials for drug delivery, in molecular imaging, and in theranostics, there are currently no nanomaterials that merge the advantages of improved efficacy with the ability to self-monitor the anticancer activity in vivo. Here we describe the design of a stimuli-responsive polymeric nanostructure, which we term a "reporter nanoparticle," comprising a polymeric backbone conjugated to a cytotoxic chemotherapeutic agent or an immunotherapy agent as an effector element and an enzyme-activatable reporter element engineered from a quenched fluorescent dye (Fig. 1). We demonstrate that such a reporter nanoparticle can start emitting a signal as early as 8 h posttreatment in the case of chemotherapy and can facilitate the distinction between responsive and resistant tumors in vivo. Additionally, it can be used to detect the efficacy of immune checkpoint inhibition at time points not accessible with current anatomic- or metabolic-based detection techniques. A reporter nanoparticle not only can emerge as a powerful platform for enhancing the efficacy of chemotherapy but additionally can provide a real-time noninvasive read out of tumor response to therapy.

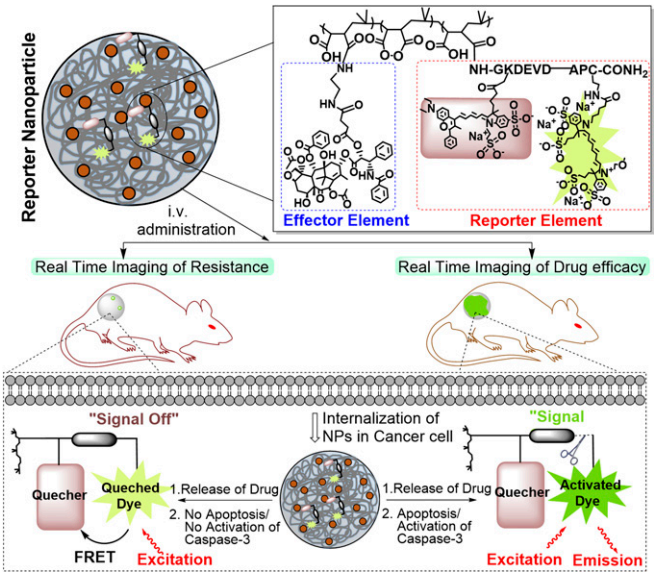

Fig. 1. Schematic showing construct of a reporter nanoparticle. The reporter nanoparticle comprises three components: a polymeric backbone, an esterase-cleavable prodrug synthesized from an anticancer drug [effector element (EE)], and an activatable reporter element (RE). At the optimal ratio of EE:RE, this stimuli-responsive polymer self-assembles into a nanoparticle. The reporter element is a caspase-3–cleavable sequence consisting of L-amino acids GKDEVDAPC-CONH2 to which we conjugated a FRET pair such that cleavage of the DEVD sequence results in removal of the quenching of the fluorescent signal. The effector element is conjugated to the polymeric backbone via an esterase-cleavable bond, whereas the reporter element is conjugated via an amide bond with the Gly residue. In normal condition, the fluorescent signal from the reporter element is in the off state because the drug is intact inside the nanoparticle. The nanoparticles home in to the tumor via the EPR effect, where the nanoparticle is internalized by cancer cell. In a drug-sensitive cell (lower right of schematic), the released drug initiates apoptosis via the activation of caspase-3 enzyme, which then cleaves the DEVD peptide, unquenching the fluorescent signal (on state). However, in a nonresponder cell (lower left), the failure of the released drug to induce apoptosis means the reporter element remains in the off state. This distinction between off and on states allows the visualization of a nanoparticle in action.

Results

Design and Synthesis of the Reporter and Effector Components of the Reporter Nanoparticle. It is well established that downstream apoptotic responses determine therapeutic outcomes (30, 31), and apoptosis defects can contribute to drug resistance (32). Similarly, the ligation of PD-L1 on cancer cells by immune checkpoint inhibitors was shown to induce apoptosis (33). Both intrinsic and extrinsic apoptotic pathways converge into caspases, a family of cysteine proteases, which are known to cleave precise substrates (34). Indeed, the activation of caspases has been extensively used to monitor cell death (35–37). We rationalized that the pathophysiological caspase activation in a drug-responsive tumor following the release of the cytotoxic effector could be used to trigger the cleavage of a quenched dye in the design of the reporter nanoparticle. The subsequent increase in the signal readout could serve as a direct real-time quantification of chemotherapy or immunotherapy efficacy (Fig. 1).

As a proof of concept, we used paclitaxel, a well-established cytotoxic chemotherapy agent that activates caspase (38), as the effector element, whereas the reporter element was designed using a short peptide containing a caspase-3–cleavable Asp-Glu-Val-Asp (DEVD) sequence inserted between either the Förster resonance energy transfer (FRET) pair of 5-FAM (visible-range fluorophore) and QSY-7 (quencher) or the pair of DyLight 755 (near-infrared fluorophore) and DyLight 766Q (quencher), where the latter pair enabled in vivo imaging. Indeed, previous studies have shown that caspase-based cleavage of the peptide bond can be used to activate fluorescence in self-quenched systems (39, 40). We used poly(isobutylene-*alt*-maleic anhydride) (PIMA), a low-molecular weight (6 kDa) polymer, as the template to engineer the stimuli-responsive material. PIMA contains reactive anhydride functional groups that can be easily conjugated to a wide range of drugs and other reactive moieties under mild reaction conditions and can be used for conjugating more than one agent for multiplexing studies. Recently, we reported that the coordination complex between platinum (II) and PIMA could enable the self-assembly into nanostructures that exhibited greater antitumor efficacy with reduced systemic toxicity compared with cisplatin (41, 42).

We first synthesized the FRET pair-based reporter element. The near-infrared (NIR) FRET pair of fluorophore, DyLight 755, and quencher, DyLight 766Q, was chosen for fabricating the reporter element for several reasons. First, Dylight 755 NIR fluorescent dye belongs to the polymethine carbocyanine family of dyes, and Dylight 766Q belongs to benzopyrillium-based quencher dyes, which have been widely used for their excellent spectral properties and biocompatibility. Second, for efficient in vivo imaging using an activatable probe for monitoring enzymatic activity, it is highly desirable to maximize signal-to-noise ratio by having no background fluorescence before and maximal fluorescence signal after activation. Hence, we used a nonfluorescent quencher, which will not have any interference post-enzymatic activation of the reporter element. Third, excellent spectral overlap of donor fluorescence (emission maxima 776 nm) and quencher absorbance (λmax 766 nm) ensured maximum quenching efficiency at 1:1 donor:acceptor ratio. Furthermore, the dyes have reactive functional groups that can be used for easy conjugation to amino acids using different bioconjugation techniques. Also, an optimum peptide length was used to conjugate the FRET pair for maximum FRET efficiency (>90%). The fluorophore and the quencher were conjugated to the caspase substrate using maleimide and amide conjugation, respectively, on either side of DEVD peptide (Fig. S1). Similarly, we synthesized a reporter element using another FRET pair consisting of a green fluorescent dye (5-FAM) and quencher QSY-7, where the quenching efficiency was 94.7% (Fig. S2). The enzymatic susceptibility of the reporter element was examined by incubating the reporter element with recombinant active caspase-3 enzyme at 37 °C and

Downloaded at Palestinian Territory, occupied on December 12, 2021
www.manaraa.com

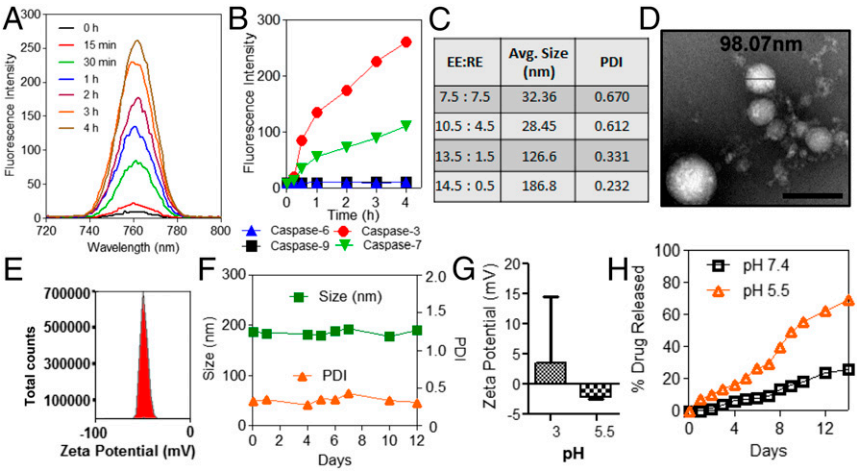

Fig. 2. Physicochemical characterization of reporter nanoparticle. (*A*) Graph shows the time-dependent activation of the reporter element (with the NIR FRET pair) in the presence of caspase-3. Reporter element (50 μM) was incubated in the presence of 50U caspase-3 enzyme at 37 °C, which results in the cleavage of the DEVD sequence and removing the quenching effect of Dylight 766Q on the fluorophore Dylight 755. The increase in fluorescence over time was monitored. (*B*) Graph shows the selective activation of the NIR-based fluorophore in reporter element by effector caspases (caspase-3 and caspase-7) compared with initiator caspases (caspase-6 and caspase-9). (*C*) Table shows the effect of optimization of ratio of the effector elements (EE) and reporter elements (RE) on the polymeric backbone on nanoparticle size and polydispersity, keeping the stimuli-responsive elements to polymer ratio of 15:1. (*D*) Representative high-resolution TEM shows the morphology and the size of the nanoparticles. (Scale bar, 200 nm.) (*E*) Graph shows zeta potential of the reporter nanoparticle at pH 7. (*F*) Graph shows the changes in size and polydispersity index (PDI) of the nanoparticles over time during storage at 4 °C as a measure of stability. (*G*) Graph shows effect of pH on zeta potential of reporter nanoparticles. (*H*) Graph shows the release kinetics profiles of paclitaxel from the nanoparticles when incubated at either pH 7.4 or 5.5. All experiments were performed in at least triplicate.

monitoring the time-dependent fluorescence activation. As shown in Fig. 2*A*, a sustained increase in the fluorescence intensity was observed with time, indicating cleavage of the peptide by the enzyme, resulting in a 31-fold increase in fluorescence intensity achieved after 4 h of incubation. Caspases are typically classified as initiators (caspase-8 and caspase-10 belonging to the extrinsic pathway and caspase-9 belonging to the intrinsic pathway) and effectors (caspase-3, caspase-6, and caspase-7), with the initiators converging into the effectors for an apoptotic outcome (43). Typically, the effectors have been shown to recognize the DEVD motif (44). To test the selectivity of different caspases for the reporter element, we incubated the reporter element with recombinant caspase-3, caspase-6, caspase-7, and caspase-9 and measured the NIR fluorescence intensity at different time points. As shown in Fig. 2*B*, caspase-3 induced the highest activation rate and preferential cleavage over caspase-7, whereas caspase-6 and caspase-9 exhibited very low activation rates, consistent with the earlier observations (44). Similar results were obtained in the case of the 5-FAM-QSY-7–based FRET pair-conjugated reporter element when incubated with caspase-3 enzyme, supporting the applicability of the reporter element platform for a series of FRET pairs with a broad emission range from green to NIR (Fig. S2).

We next synthesized the effector element by selectively conjugating a linker, 4-[(2-aminoethyl)amino]-4-oxobutanoic acid at the more reactive C-2′ OH group on the isoserine moiety of the C-13 side chain of paclitaxel (Fig. S3 *A*–*E*). Although modification of the C2 alcohol of paclitaxel is known to result in considerable loss of activity (45, 46), the use of an appropriate cleavable linker meant that the construct could be activated in the tumor cells as a result of esterase enzymatic activity. Additionally, the flexible linker of moderate length (~1 nm) was chosen so that maximum number of effector elements could be conjugated to the polymer backbone by minimizing steric hindrance. We then optimized the number of effector element molecules complexed to PIMA by studying the effect of varying polymer to effector element molar ratios on the size and stability of the self-assembled nanoparticles. As shown in Fig. S3*F*, dynamic light scattering (DLS) revealed that increasing the number of effector elements per polymer resulted in larger-size nanoparticles with a broad size distribution. At an effector element to polymer ratio of 15:1, we obtained uniform nanoparticles with a hydrodynamic diameter of 170 ± 18 nm (Fig. S3 *F* and *G*). It is well established that nanoparticles in this size range preferentially accumulate into tumors through the leaky vasculature via an enhanced permeability and retention (EPR) effect, thereby enhancing anticancer effect and reducing off-target toxicities (47).

Fabricating a Reporter Nanoparticle. We next studied the effect of varying the ratio of effector and reporter elements in the polymer construct on the nanoparticle self-assembly, while keeping the previously optimized polymer to responsive elements ratio of 1:15 constrained. As shown in Fig. 2*C*, a higher effector element to reporter element ratio resulted in nanoparticles of smaller average size but with high polydispersity index, which were stable for less than 24 h at 4 °C (Fig. S4). Nanoparticles of uniform size 186.8 ± 7.3 nm (hydrodynamic diameter) and desired stability were obtained at an optimal effector element and reporter element ratio of 14.5:0.5 per polymer (Fig. 2*C*). High-resolution transmission electron microscopy showed nanostructures of average particle size ~100 nm (Fig. 2*D*). The zeta potential of nanoparticles at pH 7.4 was measured to be −41.5 mV (Fig. 2*E*), corresponding to high colloidal stability of the reporter nanoparticles over time (Fig. 2*F*). The zeta potential of the nanoparticle was found to switch toward a more positive charge with decreasing pH (Fig. 2*G*). We next studied the release of paclitaxel from the nanoparticle as a function of pH. As shown in Fig. 2*H*, drug release was accelerated under acidic conditions. Reporter nanoparticles engineered from a 5-FAM-QSY-7–based reporter element with optimized polymer to reporter element ratio of 1:13.5 exhibited similar characteristics (Fig. S5).

In Vitro Characterization of Reporter Nanoparticle. We evaluated the in vitro efficacy of reporter nanoparticles using multiple cancer cell lines, including breast (4T1 and MDA-MB-231), ovarian (4306), and lung (LLC). As shown in Fig. 3*A*, the nanoparticles induced tumor cell kill across all of the cell lines, with IC_{50} values ranging from 217.6 ± 5.8 to 517.0 ± 4.2 nM. Although the potency of reporter nanoparticles at 48 h postincubation was lower compared with paclitaxel, we observed an increase in potency, i.e., shift of concentration–response curve to the left, with time (Fig. 3*B*), consistent with the temporal release of paclitaxel in the cells. To explore the possibility of using the reporter nanoparticles for temporal imaging of drug efficacy, we incubated cancer cells with different concentrations of reporter nanoparticles and monitored the change in fluorescence intensity. As shown in Fig. 3*C*, a concentration- and time-dependent increase in the fluorescence signal was observed, which correlated with the reduction in cell viability. Monitoring the internalization of FAM-tagged nanoparticles into the cancer cells revealed a temporal uptake of the nanoparticles

Downloaded at Palestinian Territory, occupied on December 12, 2021
www.manaraa.com

via the endolysosomal pathway (Fig. 3*D*). Furthermore, a robust overlap between the signal from the reporter (FAM-QSY7) nanoparticle and cytoplasmic active caspase-3 was noted, suggesting that the nanoparticles can escape the lysosomal compartment and the released taxane could activate the apoptotic machinery. This is consistent with previous reports where nanoparticles that switch their zeta potential from negative to positive, as observed in the current study, were shown to escape the endolysosomal compartment (48). Additionally, minimal caspase-3 and FAM signal was evident in the case of control nanoparticles that lacked an effector element, which validated that the signal observed in the case of reporter nanoparticles originates as a function of drug-induced activation of caspase-3 leading to apoptosis (Fig. 3*E*).

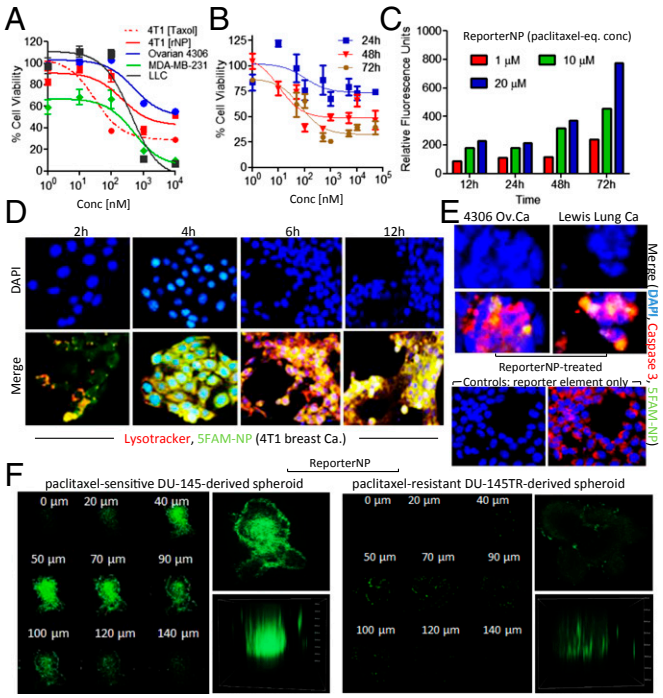

Fig. 3. In vitro validation of reporter nanoparticles. (*A*) Graph shows the log concentration effect of the reporter nanoparticle on cell viability. Different cancer cells (breast, 4T1, MDA-MB-231; ovarian, 4306; lungs, Lewis lung carcinoma) were incubated with the reporter nanoparticle (at paclitaxel-equivalent concentrations) for 48 h. Broken line represents a control group treated with paclitaxel. Cell lines exhibit different degrees of susceptibility to the reporter nanoparticle. Data are expressed relative to 100% viability in the absence of the reporter nanoparticle. (*B*) Graph shows the effect of treatment duration with reporter nanoparticles (20 μM paclitaxel-equivalent concentration) on the viability of 4T1 breast cancer cells. The shift in the concentration–response curves to the left with time is consistent to increased exposure to released drug over time. (*C*) Graph shows the effect of increasing concentration of reporter nanoparticle (paclitaxel-molar equivalent) and exposure time on the increase in fluorescent intensity, consistent with reduction in cell viability. (*D*) Representative fluorescence merge images show the internalization of 5-FAM–labeled nanoparticles at different time points in 4T1 breast cancer cells. Nuclei of the cells were labeled with DAPI (blue), and acidic endolysosomes were labeled with LysoTracker (red). The overlay indicates that the reporter nanoparticles are rapidly internalized via an endolysosomal pathway. (*E*) Representative images show that reporter nanoparticles read out caspase-3–mediated apoptosis. The 4306 ovarian cancer cells and Lewis lung carcinoma cells were incubated with FAM5-QSY7–based reporter nanoparticles. Cleaved caspase-3 was immunolabeled with rabbit mAb antibody followed by anti-rabbit Alexa Fluor 594 antibody and overlays with the activated 5-FAM signal (*Upper*). Incubating the cancer cells with a control nanoparticle with reporter element alone shows that in absence of the effector element, no FAM5 fluorescent signal is evident, and serves as controls for nonspecific activation of reporter signal (*Lower*). (*F*) Paclitaxel-sensitive (DU-145) and paclitaxel-resistant (DU-145 TR) prostate cancer cells were allowed to form spheroids, which were incubated with reporter nanoparticles (equivalent to 20 μM paclitaxel) for 24 h. The reporter nanoparticles used in this study were synthesized by using reporter element with FRET pair of 5-FAM as donor and QSY-7 as acceptor. The representative images were captured using confocal microscopy with Z-stack imaging at 10-μm intervals (all experiments were performed in triplicate). Scale bar represents 200 μm. *Left* shows the signal from the reporter nanoparticles following Z-stack reconstruction of a DU-145 spheroid after treatment with reporter nanoparticles. *Right* shows Z-stack reconstruction of DU-145TR spheroid, highlighting the absence of signal from the reporter nanoparticles in the resistant cells.

Efficiency of Reporter Nanoparticles in a 3D in Vitro System. Recent studies have shown that in vitro 3D culture systems better mimic in vivo tumor microenvironment compared with 2D monolayer cultures. Such systems model drug penetration and also conserve distinct signaling mechanisms that can influence the response to drug treatment (49, 50). We therefore treated paclitaxel-sensitive DU-145 and paclitaxel-resistant DU-145TR prostate cancer cell-derived 3D spheroids with reporter nanoparticles (at ∼20 μM paclitaxel equivalent) for 24 h. Z-stack reconstruction and images for DU145 spheroids showed activation of fluorescence signal even at a depth of 70 μm, indicating that the nanoparticles can penetrate into the core and induce cell death. In contrast, minimal signal was observed from DU-145TR spheroids, indicating that the reporter nanoparticle could distinguish between sensitive and resistant tumors. The absence of any signal from the resistant spheroids further validated the absence of nonspecific activation of the reporter element (Fig. 3*F*).

Reporter Nanoparticles Enable an Early Efficacy Readout in Vivo. To investigate if reporter nanoparticles enable the monitoring of drug response in real time in vivo, we injected multiple doses of reporter nanoparticles engineered with the NIR (Dylight)-based reporter element into 4T1 breast cancer-bearing mice and imaged the animals at different time points between the treatments (Fig. 4*A*). As shown in Fig. 4 *B*–*D*, control nanoparticles, which carried the same dose of the reporter element but no paclitaxel, exhibited baseline fluorescence inside the tumor, demonstrating that nonspecific activation of the reporter element in the tumor microenvironment was minimal and that the construct did not exhibit any toxicity to cancer cells in the absence of the cytotoxic drug. In the case of reporter nanoparticles, a significant increase in the fluorescent signal was observed as early as 8 h, but not at 4 h, after the first dose compared with control nanoparticles (Fig. 4*C* and Fig. S6 *A* and *B*). Although a reduction in the signal was evident at 24 h postadministration, subsequent injections of the reporter nanoparticles enhanced the signal, indicating a direct correlation with the presence of the drug. A detectable signal was observed even after 4 d of the last treatment, which supported the hypothesis that sustained drug release from nanoparticles can induce a prolonged apoptotic effect (Fig. 4 *C* and *D*). In contrast, it was only by day 6 that a statistically significant separation of the tumor growth curves (anatomical quantification) between the reporter nanoparticles-treated and control nanoparticles-treated group was evident (Fig. 4*E*). In earlier studies, quenched fluorescent caspase substrate-based tracers have been used to detect apoptosis in vivo (37, 51, 52). As controls, we therefore included a separate group, where the animals were treated with a combination of free paclitaxel and the reporter element at a similar dose level to that in the reporter nanoparticles. In another group, the animals were treated with a combination of an effector nanoparticle (nanoparticle with only paclitaxel) and the reporter element. In both these control groups, fluorescence signal amplification was not detected in tumors in vivo or ex vivo (Fig. 4*F* and Fig. S6 *A* and *B*). We further investigated if [^{18}F]FDG-PET/CT imaging could similarly detect the early treatment response as achieved using the reporter nanoparticles. It is well established that a decrease in FDG uptake on PET correlates with

Downloaded at Palestinian Territory, occupied on December 12, 2021
www.manaraa.com

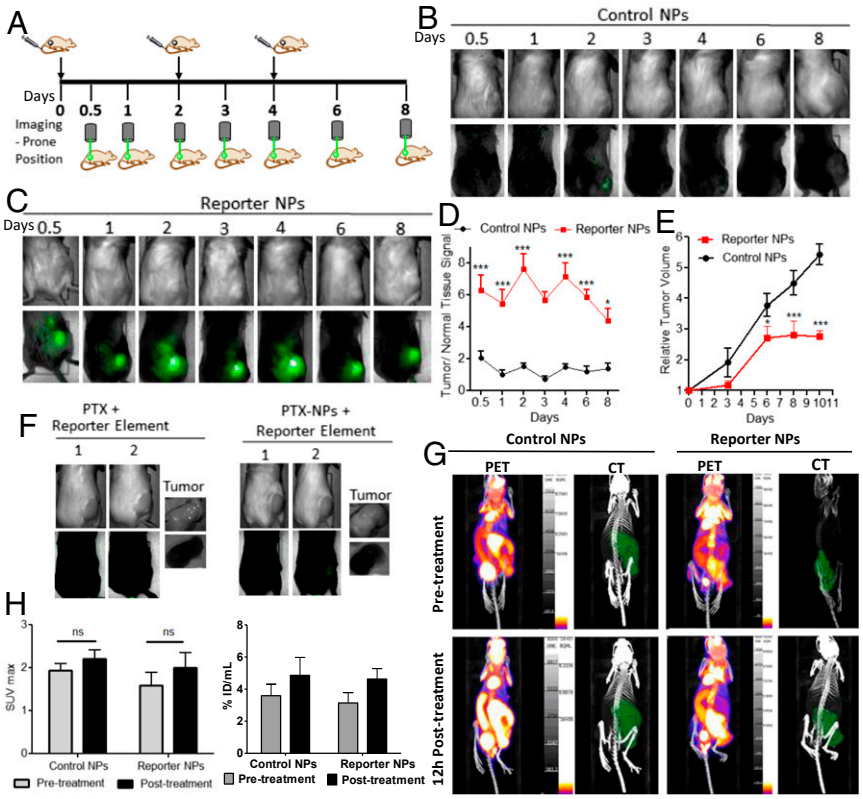

Fig. 4. Real-time reporting of drug efficacy in an in vivo syngeneic breast cancer mouse model. (*A*) A schematic showing reporter nanoparticle treatment and imaging schedule. The 4T1 breast cancer-bearing animals were injected with control nanoparticles (NPs) or reporter NPs. The control NPs were synthesized by conjugation of reporter element to the polymer backbone without paclitaxel-based effector element. When the tumor volume reached ~500 mm^3, the animals were injected with three doses of control NPs or reporter NPs (dose equivalent to 15 mg/kg paclitaxel) every alternate day (days 0, 2, and 4). The reporter element concentrations in both control NPs and reporter NPs were kept constant. The live mice imaging was done at different time points using a Maestro (CRI) in vivo fluorescence imaging system. Representative pictures from the (*B*) control NP-treated and (*C*) reporter NP-treated groups at different time points. (*D*) Graph shows the quantification of tumor response to drug treatment as measured in terms of near-infrared fluorescence intensity ratio between tumor and normal tissues at different time intervals. (*E*) Graph shows the effect of treatment on 4T1 tumor-bearing mice treated with either control NPs or reporter NPs where tumor growth was quantified as change in relative tumor volume. (*F*) Representative pictures of tumor-bearing mice imaged at 24 and 48 h after treatment with a combination of either paclitaxel (PTX) + reporter element or PTX-NP + reporter element. Side panels show ex vivo images of the tumor from the tumor bearing mice after the treatments. Lower panels capture fluorescent emission images. (*G*) [^{18}F]FDG PET and CT images of representative animals in control NPs- and reporter NPs-treated groups before and 12 h after the treatment. The 4T1 breast tumor-bearing mice were treated with reporter NPs (equivalent to 15 mg/kg of paclitaxel) or control NPs (NPs with only the reporter element). (*H*) Graphs show maximum SUV (SUV max) and % injected dose per mL (% ID/mL) for different treatment groups from the above study. Data represent mean ± SEM (n = 3–10, $^*P < 0.05$; $^{***}P < 0.001$ vs. corresponding control NP-treated values for that time point, ANOVA followed by Bonferroni's post hoc test).

a progression-free survival (7, 8). We treated animals with control nanoparticles (no effector element) or with reporter nanoparticles. However, as shown in Fig. 4 *G* and *H* and Fig. S6 *C* and *D*, we did not observe any reduction in the standard uptake value (SUV) or [^{18}F]FDG uptake in tumor at 12 h or 48 h posttreatment between control nanoparticles- and reporter nanoparticles-treated groups.

Similar results were observed when 4T1 tumor-bearing mice were treated with FAM-QSY7–based reporter nanoparticles, where ex vivo immunofluorescence imaging of tumor sections validated that the increase in antitumor efficacy correlated with an increase in caspase-3 activation and apoptosis. These results were consistent in a Lewis lung carcinoma model, although in this model, the tumor growth curves in the reporter nanoparticles- and control nanoparticles-treated groups started showing significant differences as early as after the second dose, consistent with the greater susceptibility of LLCs to the effector compared with 4T1s seen in vitro (Fig. S6 *E* and *F*).

Reporter Nanoparticles Enable Distinction Between Resistant and Sensitive Tumors in Vivo. Finally, to test if reporter nanoparticles could be used to distinguish between drug-sensitive and drug-resistant tumors in mice early on during chemotherapy, we used a dual human tumor xenograft model, where paclitaxel-sensitive (DU-145) and paclitaxel-resistant (DU-145TR) prostate cancer cells were implanted in the opposite flanks of the same mouse. The animals were injected with two doses of reporter NPs (dose equivalent to 15 mg/kg of paclitaxel) via the tail vein and imaged as previously described (Fig. 5*A*). As shown in Fig. 5 *B*–*D*, the sensitive tumor showed ~400% increase in fluorescence activation compared with resistant tumor, which was detected as early as 12 h after the first treatment. Furthermore, immunolabeling the tumor sections for cleaved caspase-3 confirmed that the mechanism of action of the reporter nanoparticle efficacy and fluorescent signal in sensitive tumor is due to drug-mediated caspase activation (Fig. 5*E*).

In a separate experiment, we studied the biodistribution of the reporter nanoparticles in tumor-bearing mice. As shown in Fig. 5*F*, we observed a preferential accumulation of the nanoparticles in the tumor, consistent with the notion that nanoparticles can home in to tumors through an EPR effect (53). We also observed significant concentrations in the liver and the kidney, which could indicate clearance routes. It should be noted that the cutoff for glomerular clearance of nanoparticles is ~5 nm (54),

Downloaded at Palestinian Territory, occupied on December 12, 2021
www.manaraa.com

indicating that the reporter nanoparticles likely break down into smaller fractions in circulation. We observed minimal accumulation in the major reticuloendothelial organs (RES), including lungs or spleen, consistent with the large hydrodynamic radii as opposed to the actual electron microscopy measurements, which means that the nanoparticles are masked from the RES.

Reporter Nanoparticles Can Be Extended to Monitoring Immunotherapy Efficacy in Vivo. We next studied whether the reporter nanoparticle can be adapted to immunotherapy. To engineer a reporter nanoparticle that acts as an immune checkpoint inhibitor, we first derivatized PIMA with different ratio of carboxy-PEG_8s. As shown in Fig. S7 *A* and *B*, at an optimal ratio of 1:10, i.e., 10 PEG_8s per molecule of PIMA, we obtained defined nanoparticles with a hydrodynamic diameter of 231 ± 22 nm, whereas higher or lower ratios resulted in particles of larger size. Using the 10:1 PEG to polymer ratio, we next conjugated the reporter element to PIMA, such that the ratio of PIMA:PEG_8:reporter element was 1:9:1. The antibody against PD-L1 was then conjugated to the PEG, resulting in nanoparticles that had a hydrodynamic diameter of 242 ± 37 nm. A control IgG-conjugated reporter nanoparticle was similarly engineered and was found to be similar in dimension as the anti-PD-L1-reporter nanoparticle. To test whether the bioconjugation conserves the binding of the antibody to PD-L1, we first treated the B16/F10 melanoma cells with IFNγ for 48 h, which resulted in an overexpression of PD-L1 compared with controls, as quantified using flow cytometry (Fig. S7*C*). These cells were then incubated with FAM-labeled reporter nanoparticles conjugated with either anti–PD-L1 antibody or control IgG. As shown in Fig. S7*D*, the anti–PD-L1-reporter nanoparticle was found to bind to the cells to a greater degree compared with the controls.

Having established the binding in vitro, we next tested whether the anti–PD-L1 reporter nanoparticles enabled the monitoring of drug response in real time in vivo. As shown in Fig. 6 *A* and *B*, compared with the IgG-control reporter nanoparticles, a significant increase in the fluorescent signal was observed by day 5 in the anti–PD-L1 reporter nanoparticles-treated group. This is consistent with the indirect mechanisms of induction of cell death following treatment with an immune checkpoint inhibitor (55). Indeed, Western blotting revealed an increased caspase activation in the cells isolated from the anti–PD-L1 reporter nanoparticles-treated tumor as opposed to the control group (Fig. 6*C*). Furthermore, quantifying $CD44^{Hi}$ $CD62L^{Lo}$ CD8+ve cells in the tumor revealed that the treatment with anti–PD-L1 reporter nanoparticles indeed enhanced activated T cell infiltration by ∼200% compared with IgG-reporter nanoparticles (Fig. 6*D*). We further investigated if [^{18}F] FDG-PET or CT imaging could similarly detect the early treatment response as achieved using the reporter nanoparticles. However, as shown in Fig. 6 *E* and *F*, we did not observe any reduction in the SUV or [^{18}F]FDG uptake in tumor even at 7 d posttreatment between control nanoparticles and reporter nanoparticles-treated groups.

Discussion

The quest for precision medicine is being driven by the development of new technologies. Here we describe the development of a reporter nanoparticle technology platform, which can preferentially deliver an anticancer treatment to the tumor and then monitor its antitumor activity in real time. Such a technology can potentially advance precision medicine by helping identify the responders and nonresponders early on while minimizing adverse effects.

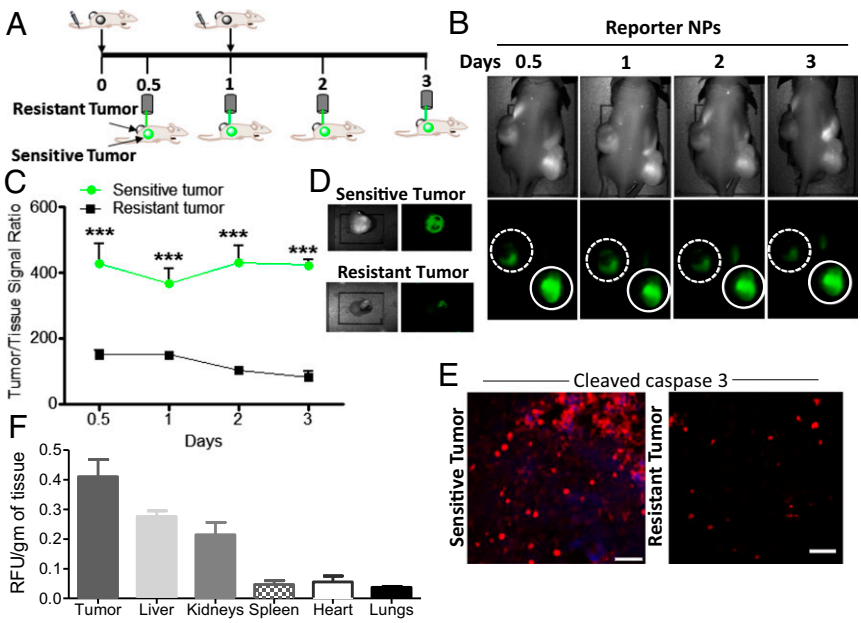

Fig. 5. Real-time imaging of drug efficacy and drug resistance in in vivo DU145 and DU-145TR dual prostate cancer BALB/c nude mice model. (*A*) Schematic shows the experimental design. Paclitaxel-sensitive and paclitaxel-resistant tumors were inoculated in the right flank and left flank of the same mice. When the tumor volume reached ∼500 mm^3, the animals were injected with two doses of reporter NPs (dose equivalent of 15 mg/kg paclitaxel). The live mice images were captured at different time points using a Maestro (CRI) in vivo fluorescence imaging system. (*B*) Representative images of sensitive (solid circle) and resistant tumors (dashed circle) from the treatment group at different time points. (*C*) Graph shows the quantification of drug response to tumor as measured in terms of near-infrared fluorescence intensity ratio between tumor and normal tissues at different time intervals. Data represent mean ± SEM ($n = 3$, $^*P < 0.05$; $^{***}P < 0.001$ vs. corresponding temporal value in resistant tumor, ANOVA followed by Bonferroni's post hoc test). (*D*) Ex vivo images of the excised tumors from the tumor bearing mice after the treatments using pseudocolor to show fluorescence emission. (*E*) Representative fluorescence images of the sections from reporter NP-treated taxane-sensitive and taxane-resistant tumors stained with a cleaved caspase-3 antibody validate the results from in vivo imaging. (*F*) Graph shows quantitative analysis of reporter-NP accumulation in different organs. Organs were excised from tumor-bearing mice 24 h after tail vein injection of NIR dye-labeled reporter NPs. Images were captured at same resolution.

PNAS PLUS
ENGINEERING
MEDICAL SCIENCES
Downloaded at Palestinian Territory, occupied on December 12, 2021
www.manaraa.com

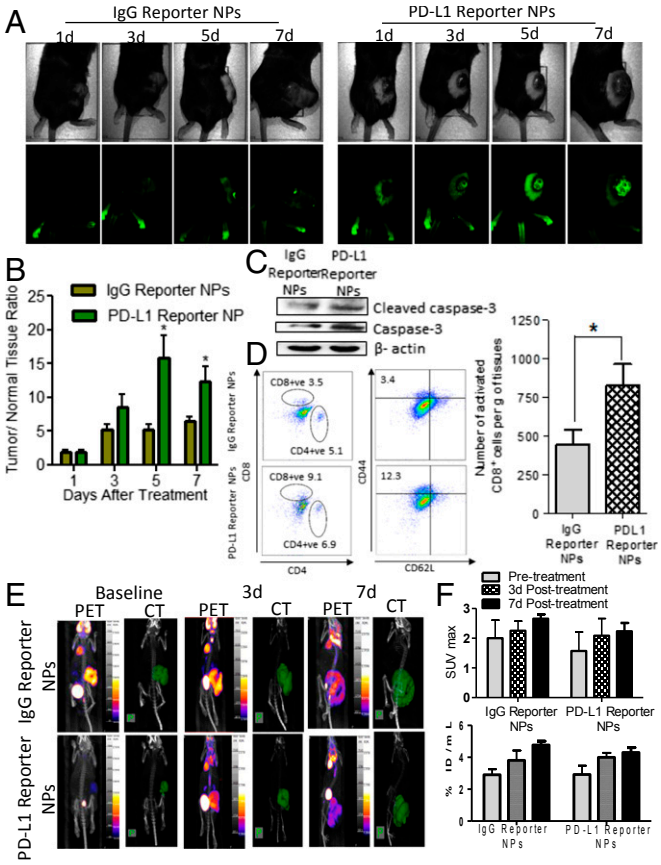

Fig. 6. Reporter nanoparticles enable imaging of immunotherapy response in a B16/F10 melanoma mouse model. (*A*) Representative images of IgG-reporter NPs and PD-L1 reporter NPs treated groups at different days after the initial treatment. The treatments were administered when the tumor volume reached ~100 mm^3, and live mice images were captured using a Maestro (CRI) in vivo fluorescence imaging system. (*B*) Graph shows the quantification of immunotherapy response to tumor as measured in terms of near infrared fluorescence intensity ratio between tumor and normal tissues at different days after the treatment. Data represent mean ± SEM ($n = 3$, $^*P < 0.05$ vs. corresponding temporal value in IgG-reporter NPs groups, ANOVA followed by Bonferroni's post hoc test). (*C*) Western blot showing expressions of caspase-3 and cleaved caspase-3 in tumors treated with different reporter NPs. (*D*) Representative FACS data from the B16/F10 tumor-bearing mice after different treatments. *Left* shows percentage of CD8+ vs. CD4+ T cells in the isolated lymphocyte population. *Right* shows the percentage of activated CD8+ T cells (CD44+ CD62L-). The graph shows quantification of number of activated CD8+ T cells per gram of tumor in different treatments. Data represent mean ± SEM ($n = 3$, $^*P < 0.05$ vs. corresponding value in IgG-reporter NPs groups; statistics was performed using Student's *t* test). (*E*) [^{18}F]FDG PET and CT images of representative animals in IgG reporter NPs- and PD-L1 reporter NPs-treated groups before and 3 and 7 d after the treatment. B16/F10 melanoma tumor-bearing mice were treated with IgG reporter NPs or PD-L1 reporter NPs. (*F*) Graphs show SUV max and % ID/mL for different treatment groups from the above study.

Although the current study builds on the recent developments in theranostics, i.e., nanomaterials comprising of a cytotoxic payload and additionally tagged with a tracer allowed the spatial visualization of nanoparticles in vivo (56, 57), such first-generation theranostic nanoparticles did not report on the efficacy of the nanoparticle-based treatment. The "always on" signal meant that these theranostic nanoparticles could not discriminate between a drug-sensitive and drug-resistant tumor. In contrast, the response-activatable aspect of the reporter nanoparticle is designed to monitor the efficacy of the nanoparticle. Indeed, our results show that the reporter nanoparticles can distinguish between a drug-sensitive and a resistant tumor. Additionally, we observed a greater tumor growth inhibition in vivo with the reporter nanoparticle as opposed to free paclitaxel. Similarly, a greater immunotherapy biomarker response in terms of TILs was observed with the PDL1-reporter nanoparticle. Previous studies have shown that cancer nanomedicines preferentially home in to tumors and as a result exert enhanced antitumor efficacy (53, 58). Indeed, the findings from our biodistribution studies are consistent with these previous reports.

Our results demonstrated that an anatomical readout of chemotherapy efficacy, i.e., changes in tumor volume, temporally lagged the quantification of apoptosis as a measure of efficacy. A reliance on the anatomical readout alone would have meant that several doses of the therapy would have been administered before we could detect the nonresponder status of a tumor. Additionally, we observed that the current clinically used techniques for monitoring efficacy, such as FDG-PET or CT, are of limited use in the acute temporal setting. In some of the animals we actually noted a transient increase in FDG uptake, consistent with the flare response seen at the onset of chemotherapy as a result of increased glucose uptake by inflammatory cells and/or energy demand of the apoptosis process (59). Additionally, recent studies have indicated that the oncogene activation status can regulate the internalization of [^{18}F]FDG (60), which can further confound the results with such imaging techniques.

The development of noninvasive molecular imaging techniques to detect apoptosis as a direct readout of chemotherapy activity is thus increasingly gaining momentum, stemming from the limitations of the current technologies in monitoring of early tumor response (61). For example, annexin V-conjugated tracers have been used to detect the exposed phosphatidylserine on the outer leaflet of the cell membrane during apoptosis (62, 63). Similarly, probes have been developed that can monitor caspase activity (35, 64–66). For example, a caspase-3–binding radiotracer, [^{18}F]ICMT-11, was recently used to study the induction of apoptosis by chemotherapeutic agents (67). Similarly, a cell-penetrating TcapQ was recently developed to improve the pharmacokinetic properties and improve delivery of FRET-based caspase probes (68). Additionally, nanoparticles have been used to detect caspase activity (69, 70). Separately, nanoparticles have been used previously to deliver paclitaxel or other cytotoxic agents (71). However, results from the current study indicate that a simple combination of two nanoparticles, one that delivers the drug and the other to detect caspase activity, is not sufficient to monitor anticancer efficacy in real time. This could potentially arise from the fact that the dynamics of apoptosis varies between the type and mechanism of action of anticancer agents and regimens and between patients, and thus, dosing the chemotherapy and the probes in the wrong temporal windows could result in erroneous conclusions about drug efficacy (67). Indeed, it is possible that such an asynchrony existed when the reporter element was coadministered separately with paclitaxel or a paclitaxel nanoparticle. Additionally, in a tumor treated with such a combination, the possibility of any cell being loaded with both elements administered separately remains a stochastic process. Although drug-induced caspase activation is a time-sensitive process, theoretically, constraining the effector and the reporter elements in a single nanostructure ensures that the reporter element is in the same cell to capture the apoptotic process initiated by the effector and thereby achieve maximal detection efficiency.

A significant finding was the possibility of using a reporter nanoparticle to deliver and monitor the efficacy of an immune checkpoint inhibitor. A major concern in immunotherapy is the systemic toxicity as a result of global activation of the immune system (72). The possibility of harnessing a nanoparticle to deliver an immunotherapeutic agent can potentially address this concern given the ability of the nanoparticle to preferentially home to the tumor. Although future studies are necessary to better elucidate this therapeutic opportunity, we did observe that the reporter

Downloaded at Palestinian Territory, occupied on December 12, 2021
www.manaraa.com

nanoparticle comprising a PD-L1 inhibitor-based effector element did mount an immunogenic response in the tumor and also bound to a greater degree on the cancer cells overexpressing PD-L1. Here we focused on monitoring the efficacy of the delivered immune checkpoint inhibitor. Consistent with the current challenges of imaging the efficacy of immunotherapy in cancer, we observed no differences in the baseline PET/CT signal and the signal from the treated groups even at day 7. In contrast, the reporter nanoparticle was able to detect the efficacy signal, although it should be noted that the detection was delayed compared with the chemotherapy-induced response, which highlights the temporal differences between the two treatments. Taken together, these results indicate that a reporter nanoparticle might emerge as a powerful technology in cancer immunotherapy.

Much of the recent advances in nanomedicines are being enabled by the development of novel stimuli-responsive materials (73). Indeed, our results indicate that the stimuli-responsive polymer-based reporter nanoparticles can efficiently deliver a chemotherapeutic agent or an immune checkpoint inhibitor to a cancer cell and capture the resulting spatiotemporal apoptotic event. The ability of the reporter nanoparticles to directly monitor kinetics of the drug-induced apoptosis process in real time, with detectable response at acute time points where current gold standards such as [^{18}F]FDG PET/CT imaging are of limited use, indicates that the reporter nanoparticles not only can enable an early readout of chemotherapy efficacy but also will be useful in monitoring emerging treatment modalities such as immunotherapy, which are associated with stromal alterations resulting in discordant metabolic flux and anatomical changes (74). A limitation of the current approach is the use of fluorescence-based detection; for clinical translation it will be necessary to design caged radiocontrast dyes that are activated by the response of the cancer cell to the effector element. In the emerging scenario of intrinsic and adaptive resistance, the ability of the reporter nanoparticles to monitor the efficacy of therapy in real time can have a major effect in the management of cancer.

Methods

Cytotoxic Reporter Nanoparticle Synthesis and Characterization. Poly(isobutylene-*alt*-maleic anhydride) (PIMA) was dissolved in Dimethylformamide (DMF). To this, 13.5× molar excess of effector element with 1.5 molar excess of reporter element (with green dye FRET pair) was added. Synthesis of effector and reporter elements is described in *SI Appendix*. To catalyze the reaction, 1,8-Diazabicyclo[5.4.0]undec-7-ene (DBU) was added. The reaction was stirred for 48 h, at room temperature, in argon atmosphere. The resulting product was dialyzed using a regenerated cellulose dialysis bag with a molecular cutoff of 3.5 kDa. The dialyzed product was then lyophilized to get a brown-colored product. For synthesis of NIR FRET pair labeled reporter nanoparticles synthesis, 1 molar equivalent of PIMA, 14.5 molar equivalent of effector element, and 0.5 molar equivalent of reporter element were used, and the reaction was performed as described above. The polymer construct conjugated with effector element and reporter element was then resuspended in double-distilled water and sonicated for 10 min to get the reporter nanoparticles. Sizing and zeta potential were quantified using a Malvern Nanozetasizer. Drug concentrations were quantified using an HPLC. The mean particle size and ζ potential of the nanoparticles was measured by Dynamic Light Scattering method using Zetasizer Nano ZS90 (Malvern). One hundred microliters of nanoparticles solution were diluted to 1 mL using DI water, and three sets of 10 measurements each were performed at 90° scattering angle to get the average particle size. The ζ potential was measured using a Zetasizer ZS90 with the nanoparticles diluted in water for measurement according to the manufacturer's manual. The morphology of the nanoparticles was measured using high-resolution TEM by phosphotungstic acid (PTA) negative staining method. The physical stability of nanoparticles was evaluated by measuring changes in mean particle size and zeta potential during storage condition at 4 °C. To quantify the loading of paclitaxel by HCl degradation assay, 1 mg of reporter nanoparticles and 2 mL of hydrochloric acid were stirred together for 6 h at 50 °C. This was followed by purification using a dichloromethane–water system. The organic layer containing the product was collected and moisture-deprived using sodium sulfate. The resultant solvent was evaporated under vacuum, and the degraded product was dissolved in acetonitrile. It was then analyzed using Analytical HPLC system (Waters). For more details, see *SI Appendix*.

Engineering an Immunotherapeutic Reporter Nanoparticle. PIMA, Carboxy-PEG, and FAM-DEVD or NIR-DEVD peptide were taken in the molar equivalent ratio (1:9:1) and dissolved in anhydrous DMF along with 20 μL of DBU and stirred under inert conditions for 48 h followed by overnight dialysis using regenerated cellulose membranes (MWCO: 100–500D) and lyophilized later. The conjugates were then resuspended in double-distilled water and sonicated for 10 min to get the nanoparticles. The 0.12 weight equivalents of IgG and PDL-1 antibodies were added separately to each of the nanoparticles along with 2 mg EDC and sulfo-NHS. The mixture was then allowed to incubate on a shaker at 4 °C overnight. The nanoparticles were then passed through a Sephadex-G-25 size exclusion column, and the size was measured by Dynamic Light Scattering method using Zetasizer Nano ZS90 (Malvern). For more details, see *SI Appendix*.

Cell Viability Assay. The 4T1 and MDA-MB-231 breast cancer cells, 4306 ovarian cancer cells, and LLC lung cancer cells were cultured in DMEM, supplemented with 10% (vol/vol) FBS and 0.1% of Antibiotic-Antimycotic 100× solution (15240-062; Invitrogen). A total of 4×10^3 cells were seeded into 96-well flat-bottomed plates. Free drug or reporter nanoparticles (normalized to equivalent amounts of free drug) were added in triplicate in each 96-well plate at appropriate concentrations and incubated in 5% CO_2 atmosphere at 37 °C. After the desired time period of incubation, cells were washed and incubated with 100 μL phenol-red free medium (without FBS) containing 20 μL of the CellTiter 96 Aqueous One Solution reagent (Promega). After 2 h incubation in a 5% CO_2 atmosphere at 37 °C, the absorbance in each well was recorded at 490 nm using an Epoch plate reader (Biotek Instruments). Blanks were subtracted from all data, and results were analyzed using GraphPad Prism software (GraphPad).

Activation of Fluorescent Dye in Reporter Element Using Caspase-3 Enzyme. Enzyme assays were performed using a fluorescence spectrophotometer (RF5120PC, Shimadzu, NA). Reporter element (0.05 mM, final concentration) was added to 1,700 μL of caspase buffer (50 mM NaCl, 50 mM Hepes, 1 mM DTT, 10 mM EDTA, 5% (vol/vol) glycerol, and 0.1% CHAPS, pH 7.2) in a cuvette at 37 °C. Fifty units of cleaved caspase-3 enzyme (AbCam) were incubated in buffer for 20 min at 37 °C. Fluorescence intensity was monitored over time with measurements recorded every 15 min using a Shimadzu Fluorescence Spectrophotometer.

Intracellular Uptake in Drug-Treated Cells. Subconfluent cells were exposed to different concentrations of reporter nanoparticles (equivalent to 1, 5, 10, and 20 μM of paclitaxel). At different time intervals starting from hour 0 to 72 h, the cells were counterstained with a Lysotracker dye and imaged using an inverted fluorescence microscope (Eclipse Ti; Nikon Instruments Inc.). Untreated cells and wells without any cells were used to account for background fluorescence.

In Vitro Apoptosis Imaging Studies. The 4T1, 4306, and LLC cells were treated with different concentrations of reporter nanoparticles for 72 h. The cells were then fixed with 4% (vol/vol) paraformaldehyde, permeabilized with saponin, and probed with rabbit mAb to cleaved caspase-3 (1:500; Cell Signaling Technology). After a series of PBS washes, the sections were probed with anti-rabbit goat mAb Alexa Fluor 594 IgG (1:500; Molecular Probes). Nucleus was stained by 4′,6-diamidino-2-phenylindole (DAPI). Images were obtained using a Nikon Eclipse Ti fluorescence microscope equipped with blue, UV, and green filters for FITC, DAPI, and caspase-3, respectively.

In Vitro Imaging Studies in Drug-Sensitive and Drug-Resistant Tumor Spheroids. Human prostate cancer cells DU-145 (paclitaxel sensitive) and DU-145 TR (paclitaxel resistant) were used to form spheroids using low binding plates as described in manufacturer's protocol (Corning). The spheroid formation was monitored by a Nikon Eclipse Inverted microscope. After the spheroid formation, reporter nanoparticles were added to the wells for 24 h. After the incubation period, the spheroids were imaged using confocal microscopy.

In Vivo Efficacy Studies in 4T1 Breast Cancer and Lewis Lung Carcinoma Model. The 4T1 breast cancer cells and Lewis lung carcinoma cells (3×10^5 cells) were implanted s.c. in the flanks of 4-wk-old BALB/c female mice and male C57BL/6 mice, respectively (weighing 20 g; Charles River Laboratories). The drug treatment was started on day 10 after tumor inoculation. The drug therapy consisted of administration of reporter nanoparticles. The formulation was

PNAS PLUS
ENGINEERING
MEDICAL SCIENCES
Downloaded at Palestinian Territory, occupied on December 12, 2021
www.manaraa.com

prepared and validated such that 100 μL of reporter nanoparticles contained 15 mg/kg of paclitaxel (administered by tail vein injection). Polymer-reporter element nanoparticles (100 μL) (without any taxanes) administered by tail vein injection were used as a control nanoparticles. The reporter nanoparticles doses were administered on the zeroth, second, and fourth days post-drug treatment. The tumor volumes were measured on every alternate day. The tumor volume was calculated by using the formula $L \times B^2$, where the longest diameter was considered as L and the shortest diameter was considered as B, as measured using a Vernier caliper. The tumors were harvested immediately following killing and stored in 10% (vol/vol) formalin or OCT frozen for further analysis. All animal procedures were approved by the Harvard Institutional Use and Care of Animals Committee.

Ex Vivo Imaging of Drug Efficacy in Lewis Lung Carcinoma Model. For imaging study, tumor slices (5 μm) were cut after being frozen in OCT medium at Harvard Medical School Core facility. For cleaved caspase-3 imaging, tumor sections were stained with primary cleaved caspase-3 antibody followed by Alexa Fluor 594 secondary antibody. For imaging of 5-FAM dye after cleavage of peptide, the tumor sections were imaged using FITC filter. For TUNEL imaging studies, tumor sections were stained with standard TMR red fluorescent terminal deoxynucleotidyl tranferase-mediated dUTP nick end labeling (TUNEL) kit following the manufacturer's protocol (In Situ Cell Death Detection Kit, TMR-Red; Roche). Images were obtained using a Nikon Eclipse TE2000 fluorescence microscope equipped with red filter.

In Vivo Imaging of Drug Efficacy and Toxicity in 4T1 Breast Cancer Model. The 4T1 breast cancer cells (3×10^5 cells) were implanted s.c. in the flanks of 4-wk-old BALB/c female mice (weighing ∼20 g; Charles River Laboratories). The drug treatment was started on day 10 after tumor inoculation. The drug therapy consisted of administration of reporter nanoparticles. The formulation was prepared and validated such that 100 μL of reporter nanoparticles contained the NIR FRET pair, DyLight 755 dye and DyLight 766 quencher-based reporter element, and the effector element containing a paclitaxel-equivalent dose of 15 mg/kg (administered via tail vein injection). At desired time points after injections, the in vivo NIR fluorescence images were captured using a Maestro (CRI) in vivo fluorescence imaging system. For details of the imaging, please refer to *SI Appendix*. Fluorescence signals were normalized and quantified using Maestro Software. The Maestro Software was used to conduct spectral unmixing. All animal procedures were approved by the Harvard Institutional Use and Care of Animals Committee.

In Vivo Imaging of Drug Efficacy and Drug Resistance in Dual Tumor Model. DU15 prostate cancer cells (1.5×10^6 cells) and DU145 TR paclitaxel-resistant prostate cancer cells (3×10^6 cells) were inoculated in Matrigel (BD Biosciences) in the right and left flanks, respectively, of 4- to 5-wk-old male BALB/c athymic nude mice. The drug treatment with reporter nanoparticles was started when the tumor volume reached 500 mm^3. The formulation was prepared and validated such that 100 μL of reporter nanoparticles contained 15 mg/kg of paclitaxel (administered i.v.). At desired time points after injections, the in vivo NIR fluorescence images were taken using Maestro (CRI) in vivo fluorescence imaging system.

PET/CT Scanning. All mice were anesthetized using isoflurane for the radioisotope injection, as well as for the duration of the imaging procedure. A customary protocol for PET imaging was performed, where 0.350–0.400 mCi FDG-F18 was injected retroorbitally 1 h before imaging on the NanoPET/CT (Mediso). Following a 1-h postinjection period, the mice were imaged at the Longwood Small Animal Imaging Facility. PET/CT imaging was performed using a Minerve anesthesia bed on a NanoPET/CT imaging system. First, a 30-min whole body FDG-PET scan was acquired. Following the PET scan, the mice received a 10-min whole-body CT scan on the same instrument. The acquisition software used for all scans was Nucline v1.07 (inviCRO). Counts per minute were obtained and were converted to Bq. To normalize for variability in injected dose, mouse weight, and tumor specific uptake changes, the SUV was calculated using the following formula: (mean activity in tumor in Bq)/(injected activity in Bq)/(mouse weight). All analysis was done on Vivoquant software (inviCRO).

Study of PDL-1 Nanoparticle Internalization in B16 F10 Melanoma Cells in Vitro. B16 F10 melanoma cells were seeded in a density of 100,000 cells per well in a six-well plate and made to overexpress PDL-1 on their surface by treatment with 100 ng/mL IFN-γ for 48 h. The PIMA-carboxy PEG-FAM DEVD peptide nanoparticles coated with PDL-1 antibody were added to the cells at a final concentration of 25 μM. After 4 h the media was aspirated, and the cells were washed with cold PBS and were collected for flow cytometric analysis. PIMA-carboxy-PEG-FAM DEVD nanoparticles coated with IgG were used as control. FACS analysis was done using FlowJo.

In Vivo Monitoring of Immunotherapy Response in B16F10 Melanoma Model Using Reporter Nanoparticles. The B16F10 melanoma cells (5×10^5 cells) were implanted s.c. in the flanks of 4-wk-old C57BL/6 male mice (weighing ∼20 g; Charles River Laboratories). The drug treatment was started on day 10 after tumor inoculation. The drug therapy consisted of administration of PD-L1 reporter NPs and control IgG reporter NPs. The formulation was prepared and validated such that 100 μL of reporter nanoparticles contained the NIR FRET pair, DyLight 755 dye and DyLight 766 quencher-based reporter element, and the effector element containing a PD-L1–equivalent dose of 5 mg/kg (administered via tail vein injection). Control IgG reporter NPs contained same equivalents of reporter element and antibody concentration. Additionally, 10 mg/kg of anti–PD-L1 antibody was injected along with PD-L1 reporter NP. At desired time points after injections, the in vivo NIR fluorescence images were captured using a Maestro (CRI) in vivo fluorescence imaging system. In additional groups treated with PD-L1 reporter NPs and IgG reporter NPs, PET/CT imaging was performed at desired time points. Fluorescence signals were normalized and quantified using Maestro Software. The Maestro Software was used to conduct spectral unmixing. All animal procedures were approved by the Harvard Institutional Use and Care of Animals Committee.

Flow Cytometric Analysis to Study in Vivo T Cell Infiltration. Mice treated with IgG and PDL-1 coated nanoparticles were killed 7 d posttreatment. The tumors were then excised and homogenized in serum-free RPMI-1640 media containing 175U/mL collagenase type I, into a single cell suspension. The T cells were then isolated using Mouse CD90.2 positive selection kit and stained with APC anti-mouse CD4 and FITC anti-mouse CD8a antibodies to study the populations of CD4+ve and CD8+ve T cells. Activated CD8+ve T cell populations were studied by staining the cells with APC Rat anti-mouse CD62L and FITC Rat anti-mouse CD44 antibodies. Antibody dilutions and isotype controls were used according to manufacturer's protocols.

Western Blot for Showing Expression of Cleaved Caspase-3 in in Vivo Samples. Tumor samples from mice were homogenized and lysed in Nonidet P-40 cell lysis buffer containing protease and phosphatase inhibitors. The cellular debris was removed by centrifugation at 20,800 × *g*, and the supernatant was taken for the experiment. Protein estimation was done by BCA protein assay kit. Thirty micrograms of protein was loaded in each well and probed for caspase-3, cleaved caspase-3, and beta actin proteins. The blot was imaged by G-Box, Syngene.

Statistics. The statistical analysis was determined by two-tailed Student's *t* test and one-way ANOVA followed by Bonferroni's post hoc test. $P < 0.05$ indicated a significant difference.

ACKNOWLEDGMENTS. S.S. is supported by a Department of Defense (DoD) Breast Cancer Research Program Collaborative Innovator Grant (W81XWH-09-1-0700), National Institutes of Health Grant R01 (1R01CA135242), a DoD Breakthrough Award (BC132168), and an American Lung Association Innovation Award (LCD-259932-N). A.G. is supported by an American Cancer Society Postdoctoral Fellowship (122854-PF-12-226-01-CDD).

1. Majumder B, et al. (2015) Predicting clinical response to anticancer drugs using an ex vivo platform that captures tumour heterogeneity. *Nat Commun* 6:6169.
2. Marusyk A, Almendro V, Polyak K (2012) Intra-tumour heterogeneity: A looking glass for cancer? *Nat Rev Cancer* 12(5):323–334.
3. Kreso A, et al. (2013) Variable clonal repopulation dynamics influence chemotherapy response in colorectal cancer. *Science* 339(6119):543–548.
4. Goldman A, et al. (2015) Temporally sequenced anticancer drugs overcome adaptive resistance by targeting a vulnerable chemotherapy-induced phenotypic transition. *Nat Commun* 6:6139.
5. Avril N, Sassen S, Roylance R (2009) Response to therapy in breast cancer. *J Nucl Med* 50(Suppl 1):55S–63S.
6. Cunningham D, et al. (2004) Cetuximab monotherapy and cetuximab plus irinotecan in irinotecan-refractory metastatic colorectal cancer. *N Engl J Med* 351(4):337–345.
7. Groheux D (2014) Predicting pathological complete response in breast cancer early. *Lancet Oncol* 15(13):1415–1416.
8. Harry VN, Semple SI, Parkin DE, Gilbert FJ (2010) Use of new imaging techniques to predict tumour response to therapy. *Lancet Oncol* 11(1):92–102.
9. Pfannenberg C, et al. (2010) PET/CT with 18F-FLT: Does it improve the therapeutic management of metastatic germ cell tumors? *J Nucl Med* 51(6):845–853.
10. Ruers TJ, et al. (2002) Value of positron emission tomography with [F-18]fluorodeoxyglucose in patients with colorectal liver metastases: A prospective study. *J Clin Oncol* 20(2):388–395.

Downloaded at Palestinian Territory, occupied on December 12, 2021
www.manaraa.com

11. Chiou VL, Burotto M (2015) Pseudoprogression and immune-related response in solid tumors. *J Clin Oncol* 33(31):3541–3543.
12. Scheinberg DA, Villa CH, Escorcia FE, McDevitt MR (2010) Conscripts of the infinite armada: Systemic cancer therapy using nanomaterials. *Nat Rev Clin Oncol* 7(5):266–276.
13. Sengupta S, Sasisekharan R (2007) Exploiting nanotechnology to target cancer. *Br J Cancer* 96(9):1315–1319.
14. Sengupta S, Tyagi P, Chandra S, Kochupillai V, Gupta SK (2001) Encapsulation in cationic liposomes enhances antitumour efficacy and reduces the toxicity of etoposide, a topo-isomerase II inhibitor. *Pharmacology* 62(3):163–171.
15. Sengupta S, Kulkarni A (2013) Design principles for clinical efficacy of cancer nanomedicine: A look into the basics. *ACS Nano* 7(4):2878–2882.
16. Sengupta P, et al. (2012) Cholesterol-tethered platinum II-based supramolecular nanoparticle increases antitumor efficacy and reduces nephrotoxicity. *Proc Natl Acad Sci USA* 109(28):11294–11299.
17. Kulkarni AA, et al. (2013) Supramolecular nanoparticles that target phosphoinositide-3-kinase overcome insulin resistance and exert pronounced antitumor efficacy. *Cancer Res* 73(23):6987–6997.
18. Sengupta S, et al. (2005) Temporal targeting of tumour cells and neovasculature with a nanoscale delivery system. *Nature* 436(7050):568–572.
19. Chow EK, Ho D (2013) Cancer nanomedicine: From drug delivery to imaging. *Sci Transl Med* 5(216):216rv4.
20. Weissleder R, Ntziachristos V (2003) Shedding light onto live molecular targets. *Nat Med* 9(1):123–128.
21. Qian X, et al. (2008) In vivo tumor targeting and spectroscopic detection with surface-enhanced Raman nanoparticle tags. *Nat Biotechnol* 26(1):83–90.
22. Li C (2014) A targeted approach to cancer imaging and therapy. *Nat Mater* 13(2): 110–115.
23. Will O, et al. (2006) Diagnostic precision of nanoparticle-enhanced MRI for lymph-node metastases: A meta-analysis. *Lancet Oncol* 7(1):52–60.
24. Zhang G, Palmer GM, Dewhirst MW, Fraser CL (2009) A dual-emissive-materials design concept enables tumour hypoxia imaging. *Nat Mater* 8(9):747–751.
25. Wang Y, et al. (2014) A nanoparticle-based strategy for the imaging of a broad range of tumours by nonlinear amplification of microenvironment signals. *Nat Mater* 13(2): 204–212.
26. Olson ES, et al. (2010) Activatable cell penetrating peptides linked to nanoparticles as dual probes for in vivo fluorescence and MR imaging of proteases. *Proc Natl Acad Sci USA* 107(9):4311–4316.
27. Lee GY, et al. (2013) Theranostic nanoparticles with controlled release of gemcitabine for targeted therapy and MRI of pancreatic cancer. *ACS Nano* 7(3):2078–2089.
28. Veiseh O, Gunn JW, Zhang M (2010) Design and fabrication of magnetic nanoparticles for targeted drug delivery and imaging. *Adv Drug Deliv Rev* 62(3):284–304.
29. Samuelson LE, Scherer RL, Matrisian LM, McIntyre JO, Bornhop DJ (2013) Synthesis and in vitro efficacy of MMP9-activated NanoDendrons. *Mol Pharm* 10(8):3164–3174.
30. Schmitt CA, et al. (2002) Dissecting p53 tumor suppressor functions in vivo. *Cancer Cell* 1(3):289–298.
31. Schmitt CA, Lowe SW (2002) Apoptosis and chemoresistance in transgenic cancer models. *J Mol Med (Berl)* 80(3):137–146.
32. Pommier Y, Sordet O, Antony S, Hayward RL, Kohn KW (2004) Apoptosis defects and chemotherapy resistance: Molecular interaction maps and networks. *Oncogene* 23(16):2934–2949.
33. Martínez-Lostao L, Anel A, Pardo J (2015) How do cytotoxic lymphocytes kill cancer cells? *Clin Cancer Res* 21(22):5047–5056.
34. Johnson CE, Kornbluth S (2008) Caspase cleavage is not for everyone. *Cell* 134(5): 720–721.
35. Edgington LE, et al. (2009) Noninvasive optical imaging of apoptosis by caspase-targeted activity-based probes. *Nat Med* 15(8):967–973.
36. Bullok K, Piwnica-Worms D (2005) Synthesis and characterization of a small, membrane-permeant, caspase-activatable far-red fluorescent peptide for imaging apoptosis. *J Med Chem* 48(17):5404–5407.
37. Maxwell D, Chang Q, Zhang X, Barnett EM, Piwnica-Worms D (2009) An improved cell-penetrating, caspase-activatable, near-infrared fluorescent peptide for apoptosis imaging. *Bioconjug Chem* 20(4):702–709.
38. Oyaizu H, et al. (1999) A crucial role of caspase 3 and caspase 8 in paclitaxel-induced apoptosis. *Mol Cell Biol Res Commun* 2(1):36–41.
39. Motoi Oishi AT, Nakamura T, Nagasaki Y (2009) A smart nanoprobe based on fluorescence-quenching PEGylated nanogels containing gold nanoparticles for monitoring the response to cancer therapy. *Adv Funct Mater* 19(6):827–834.
40. Peng X, et al. (2009) A nonfluorescent, broad-range quencher dye for Förster resonance energy transfer assays. *Anal Biochem* 388(2):220–228.
41. Paraskar AS, et al. (2010) Harnessing structure-activity relationship to engineer a cisplatin nanoparticle for enhanced antitumor efficacy. *Proc Natl Acad Sci USA* 107(28):12435–12440.
42. Paraskar A, et al. (2011) Rationally engineered polymeric cisplatin nanoparticles for improved antitumor efficacy. *Nanotechnology* 22(26):265101.
43. Degterev A, Boyce M, Yuan J (2003) A decade of caspases. *Oncogene* 22(53): 8543–8567.
44. Smith BA, Smith BD (2012) Biomarkers and molecular probes for cell death imaging and targeted therapeutics. *Bioconjug Chem* 23(10):1989–2006.
45. Kingston DGI (2000) Recent advances in the chemistry of taxol. *J Nat Prod* 63(5): 726–734.
46. Dubikovskaya EA, Thorne SH, Pillow TH, Contag CH, Wender PA (2008) Overcoming multidrug resistance of small-molecule therapeutics through conjugation with releasable octaarginine transporters. *Proc Natl Acad Sci USA* 105(34):12128–12133.
47. Banerjee D, Sengupta S (2011) Nanoparticles in cancer chemotherapy. *Prog Mol Biol Transl Sci* 104:489–507.
48. Panyam J, Zhou WZ, Prabha S, Sahoo SK, Labhasetwar V (2002) Rapid endo-lysosomal escape of poly(DL-lactide-co-glycolide) nanoparticles: Implications for drug and gene delivery. *FASEB J* 16(10):1217–1226.
49. Friedrich J, Seidel C, Ebner R, Kunz-Schughart LA (2009) Spheroid-based drug screen: Considerations and practical approach. *Nat Protoc* 4(3):309–324.
50. Sengupta S, Kiziltepe T, Sasisekharan R (2004) A dual-color fluorescence imaging-based system for the dissection of antiangiogenic and chemotherapeutic activity of molecules. *FASEB J* 18(13):1565–1567.
51. Zhang Z, et al. (2009) Activatable molecular systems using homologous near-infrared fluorescent probes for monitoring enzyme activities in vitro, in cellulo, and in vivo. *Mol Pharm* 6(2):416–427.
52. Kobayashi H, Choyke PL (2011) Target-cancer-cell-specific activatable fluorescence imaging probes: Rational design and in vivo applications. *Acc Chem Res* 44(2):83–90.
53. Davis ME, Chen ZG, Shin DM (2008) Nanoparticle therapeutics: An emerging treatment modality for cancer. *Nat Rev Drug Discov* 7(9):771–782.
54. Choi HS, et al. (2007) Renal clearance of quantum dots. *Nat Biotechnol* 25(10): 1165–1170.
55. Topalian SL, Drake CG, Pardoll DM (2015) Immune checkpoint blockade: A common denominator approach to cancer therapy. *Cancer Cell* 27(4):450–461.
56. Kim K, et al. (2010) Tumor-homing multifunctional nanoparticles for cancer theragnosis: Simultaneous diagnosis, drug delivery, and therapeutic monitoring. *J Control Release* 146(2):219–227.
57. Choi KY, Liu G, Lee S, Chen X (2012) Theranostic nanoplatforms for simultaneous cancer imaging and therapy: Current approaches and future perspectives. *Nanoscale* 4(2):330–342.
58. Peer D, et al. (2007) Nanocarriers as an emerging platform for cancer therapy. *Nat Nanotechnol* 2(12):751–760.
59. Ueda S, T Saeki (2013) Early prediction of tumor response: A future strategy for optimizing cancer treatment. *Positron Emission Tomography - Recent Developments in Instrumentation, Research and Clinical Oncological Practice*, ed Misciagna S (InTech, Rijeka, Croatia), pp 257–274.
60. Alvarez JV, et al. (2014) Oncogene pathway activation in mammary tumors dictates FDG-PET uptake. *Cancer Res* 74(24):7583–7598.
61. Haberkorn U, Markert A, Mier W, Askoxylakis V, Altmann A (2011) Molecular imaging of tumor metabolism and apoptosis. *Oncogene* 30(40):4141–4151.
62. Schellenberger EA, et al. (2002) Annexin V-CLIO: A nanoparticle for detecting apoptosis by MRI. *Mol Imaging* 1(2):102–107.
63. Kartachova MS, et al. (2008) 99mTc-HYNIC-rh-annexin-V scintigraphy: Visual and quantitative evaluation of early treatment-induced apoptosis to predict treatment outcome. *Nucl Med Commun* 29(1):39–44.
64. Hight MR, et al. (2014) A peptide-based positron emission tomography probe for in vivo detection of caspase activity in apoptotic cells. *Clin Cancer Res* 20(8):2126–2135.
65. Neves AA, Brindle KM (2014) Imaging cell death. *J Nucl Med* 55(1):1–4.
66. Ye D, et al. (2014) Bioorthogonal cyclization-mediated in situ self-assembly of small-molecule probes for imaging caspase activity in vivo. *Nat Chem* 6(6):519–526.
67. Nguyen QD, et al. (2013) Temporal and spatial evolution of therapy-induced tumor apoptosis detected by caspase-3-selective molecular imaging. *Clin Cancer Res* 19(14): 3914–3924.
68. Barnett EM, Zhang X, Maxwell D, Chang Q, Piwnica-Worms D (2009) Single-cell imaging of retinal ganglion cell apoptosis with a cell-penetrating, activatable peptide probe in an in vivo glaucoma model. *Proc Natl Acad Sci USA* 106(23):9391–9396.
69. Kim K, et al. (2006) Cell-permeable and biocompatible polymeric nanoparticles for apoptosis imaging. *J Am Chem Soc* 128(11):3490–3491.
70. Sun IC, et al. (2010) Caspase sensitive gold nanoparticle for apoptosis imaging in live cells. *Bioconjug Chem* 21(11):1939–1942.
71. Koziara JM, Whisman TR, Tseng MT, Mumper RJ (2006) In-vivo efficacy of novel paclitaxel nanoparticles in paclitaxel-resistant human colorectal tumors. *J Control Release* 112(3):312–319.
72. Gangadhar TC, Vonderheide RH (2014) Mitigating the toxic effects of anticancer immunotherapy. *Nat Rev Clin Oncol* 11(2):91–99.
73. Ganta S, Devalapally H, Shahiwala A, Amiji M (2008) A review of stimuli-responsive nanocarriers for drug and gene delivery. *J Control Release* 126(3):187–204.
74. Wolchok JD, et al. (2009) Guidelines for the evaluation of immune therapy activity in solid tumors: Immune-related response criteria. *Clin Cancer Res* 15(23):7412–7420.

Downloaded at Palestinian Territory, occupied on December 12, 2021

www.manaraa.com